Electron–Swirl Coupled Transport in Swirl–String Theory (SST): Perturbative Solutions, Quantitative Benchmarks, and Falsifiable Experiments

Omar Iskandarani

*Independent Researcher, Groningen, The Netherlands**

(Dated: January 27, 2026)

Abstract

I present a self-contained treatment of electron–swirl transport within *Swirl–String Theory (SST)*. The analysis (i) derives a *perturbative, steady-state* solution to the coupled density-matrix equations in 1D, (ii) makes *quantitative* predictions for tabletop experiments with explicit materials, geometries, and signal levels, and (iii) states clear *falsifiability criteria*. The framework reproduces the Peierls (population) and Allen–Feldman (coherence) limits [1–3] while embedding electrons as *swirl strings* (knotted vortex filaments) coupled to swirl modes. Kinematic time-rate variations locally modulate the electronic Hamiltonian through the *Swirl Clock* factor [4, 5]. The swirl clock $\S_t^{\circlearrowleft}$ corresponds to a scalar time-foliation field (khronon) whose gradient defines the local time direction, analogous to the preferred foliation in Einstein–Æther and Hořava–Lifshitz gravity [18, 19]. Numerical scales are anchored by SST canonical values $\mathbf{v}_{\circlearrowleft} = 1.09384563 \times 10^6 \,\mathrm{m/s}$, $r_c = 1.40897017 \times 10^{-15}\,\mathrm{m}$, and $\rho_f = 7.0 \times 10^{-7}\,\mathrm{kg/m^3}$. For compactness, some intermediate results are given in units of the SST frequency Ω_0; all final predictions are reported in SI units.

Authorial note. — This is a single-author work; I use "we" in the conventional authorial sense in the derivations and exposition that follow.

I.   SCALES FROM SST

SST fixes a characteristic core-swirl frequency and an associated energy density,

$$\Omega_0 \equiv \frac{\mathbf{v}_{\circlearrowleft}}{r_c} \approx 7.76 \times 10^{20}\,\mathrm{s^{-1}}, \qquad \rho_E \equiv \tfrac{1}{2}\,\rho_f\,\mathbf{v}_{\circlearrowleft}^2 \approx 4.19 \times 10^5\,\mathrm{J/m^3}. \tag{1}$$

When it aids readability, rates are reported in Ω_0 units; conversion uses $r_{\mathrm{SI}} = \hat{r}\,\Omega_0$ and $\tau_{\mathrm{SI}} = \hat{\tau}/\Omega_0$ (see App. C.3). Spatial gradients in the Swirl Clock act as a multiplicative modulation in the electronic Hamiltonian H_e and do not change how observables are reported in SI.

Operationally, spatial gradients in the Swirl Clock produce local kinematic time-rate variations. These enter the electronic Hamiltonian H_e multiplicatively as a modulation factor and do not alter the SI reporting of observables. Where it improves readability, I normalize rates to Ω_0; experimental benchmarks and error budgets remain in SI.

Roadmap. Section IV states the falsifiability logic up front and defines the chirality null test. Section II derives the 1D coupled transport and the coherence term in κ; Sec. III links $\Delta\kappa/\kappa$ to a measurable $\Delta(\Delta T)$ in a bar. Section IV gives quantitative benchmarks and device recipes. Appendices collect the operator content and scalings (App. A), the null-test derivation and layouts (App. B), and the SST ontology, clock, and $\Omega_0 \leftrightarrow$SI map (App. C).

II. COUPLED TRANSPORT IN 1D AND PERTURBATIVE SOLUTION

We adapt the unified density-matrix framework for bosons $N(\mathbf{R}, \mathbf{q})$ [3] to a charged two-level "electron" with density matrix f, coupled in the Born–Markov rotating-wave limit:

$$\partial_t N = -i[\Omega, N] - \Gamma_{\mathrm{b}} \circ (N - N^{(0)}) - \tfrac{1}{2}\{V_x \partial_x, N\}, \tag{2}$$

$$\partial_t f = -i[H_e, f] - \Gamma_{\mathrm{e}} \circ (f - f^{(0)}) - \tfrac{1}{2}\{v_{e,x}\partial_x, f\} + \mathcal{C}_{e\leftrightarrow b}, \tag{3}$$

$$\mathcal{C}_{e\leftrightarrow b} \equiv -\frac{i}{\hbar}[M, f\otimes N]_{\mathrm{RWA}}.$$

For a small, uniform $\partial_x T$ and a time-independent state, we linearize around $N^{(0)}(T)$ and $f^{(0)}(T)$. In a near-degenerate two-branch bosonic subspace s, s' with detuning $\delta = \Omega_{s'} - \Omega_s$ and one electronic transition Δ, the off-diagonal coherence obeys

$$\mathcal{C}_{e\leftrightarrow b} \equiv -\frac{i}{\hbar}[M, f \otimes N]_{\mathrm{RWA}}. \tag{4}$$

A. Linear response to a static gradient

Consider a small uniform temperature gradient $\partial_x T$ and a time-independent steady state. Linearize about $N^{(0)}(T)$ and $f^{(0)}(T)$ via $N = N^{(0)} + N^{(1)}$ and $f = f^{(0)} + f^{(1)}$, retaining $\mathcal{O}(\partial_x T)$ terms. For a *two-branch* bosonic subspace s, s' that interacts through $\boldsymbol{\omega}_5$ and is near-degenerate by $\delta = \Omega_{s'} - \Omega_s$, with a single electronic transition Δ, the off-diagonal coherence $N_{ss'}^{(1)}$ obeys

$$\left[i\delta + \tfrac{1}{2}(\gamma_s + \gamma_{s'})\right] N_{ss'}^{(1)} = -\frac{1}{2}V_{ss'}^{(x)}\partial_x N_{\mathrm{pop}}^{(0)}(\Omega) - \frac{i}{\hbar}\Xi_{ss'}, \tag{5}$$

where γ are the linewidths and $\Xi_{ss'}$ is the electron-induced source from $\mathcal{C}_{e\leftrightarrow b}$ (proportional to the vertex M and to $f^{(1)}$). The population correction satisfies

$$\gamma_s N_{ss}^{(1)} + V_{ss}^{(x)}\partial_x N_{ss}^{(0)} + 2\,\mathrm{Im}\big(V_{ss'}^{(x)} N_{s's}^{(1)}\big) = S_s^{(e)}, \tag{6}$$

with $S_s^{(e)}$ collecting the remaining electron-related terms.

B.   Closed form for the coherence contribution to κ

The heat current density for bosonic modes is $J_x = \text{Tr}\big[\{V_x, N\}\,\Omega/2\big]$ [3, 6]. Using Eqs. (5)–(6) and eliminating $f^{(1)}$ in the weak-coupling (Born) limit yields the *coherence* part of the 1D thermal conductivity

$$\kappa_{1D}^{(C)} = \sum_q \sum_{s \neq s'} \frac{(\Omega_s + \Omega_{s'})\,\Gamma_{ss'}\,|V_{ss'}^{(x)}|^2}{4\delta^2 + \Gamma_{ss'}^2}\left(-\frac{\partial n_B}{\partial T}\right) + \mathcal{O}(|M|^2)\,, \tag{7}$$

with $\Gamma_{ss'} = \frac{1}{2}(\gamma_s + \gamma_{s'})$ and n_B the Bose function. Equation (7) reduces to Peierls (no off-diagonals) and to Allen–Feldman (flat bands, $V_{ss} \to 0$) in the appropriate limits [1–3]. The $\mathcal{O}(|M|^2)$ terms add an *electron-assisted* channel that shares the Lorentzian denominator and peaks at small detuning.

III.   1D SLAB: TEMPERATURE FIELD AND $\Delta\kappa/\kappa$

For a bar of length L, cross-section A, and conductivity $\kappa = \kappa^{(P)} + \kappa^{(C)}$, a steady power P at $x = 0$ with a sink at $x = L$ sets

$$\partial_x T = -\frac{P}{\kappa A}, \qquad \Delta T \equiv T(0) - T(L) = \frac{P\,L}{\kappa A}. \tag{8}$$

A small change $\Delta\kappa$ gives

$$\Delta(\Delta T) \approx -\frac{\Delta\kappa}{\kappa}\,\Delta T\,, \tag{9}$$

which ties the measured temperature drop directly to δ, Γ, and $V_{ss'}$ through Eq. (7).

IV.   FALSIFIABILITY AND A CHIRALITY NULL TEST

The electron–swirl interpretation is *falsified* under the stated drive if any of the following hold:

1. **Missing detuning peak.** At fixed current, $\Delta\kappa(\delta)$ lacks the Lorentzian kernel $\propto (4\delta^2 + \Gamma^2)^{-1}$ of Eq. (7).

2. **No chirality asymmetry.** Define $\Delta\kappa_{\text{asym}} \equiv [\Delta\kappa]_{\to} - [\Delta\kappa]_{\leftarrow}$. Reversing the 3-phase sequence $(0, 120°, 240°) \leftrightarrow (0, 240°, 120°)$ must flip $\text{sgn}(\Delta\kappa_{\text{asym}})$ within 3σ; failure to invert the sign falsifies a chiral coupling (App. B.3).

3. **Scaling mismatch.** The signal fails to scale as $|V_{ss'}^{(x)}|^2$ (coil-current squared) or fails to track Γ under controlled disorder.

Operator structure and rate scaling for electron assistance are summarized in App. A; electron ontology/clock and $\Omega_0 \leftrightarrow SI$ mapping in App. C.
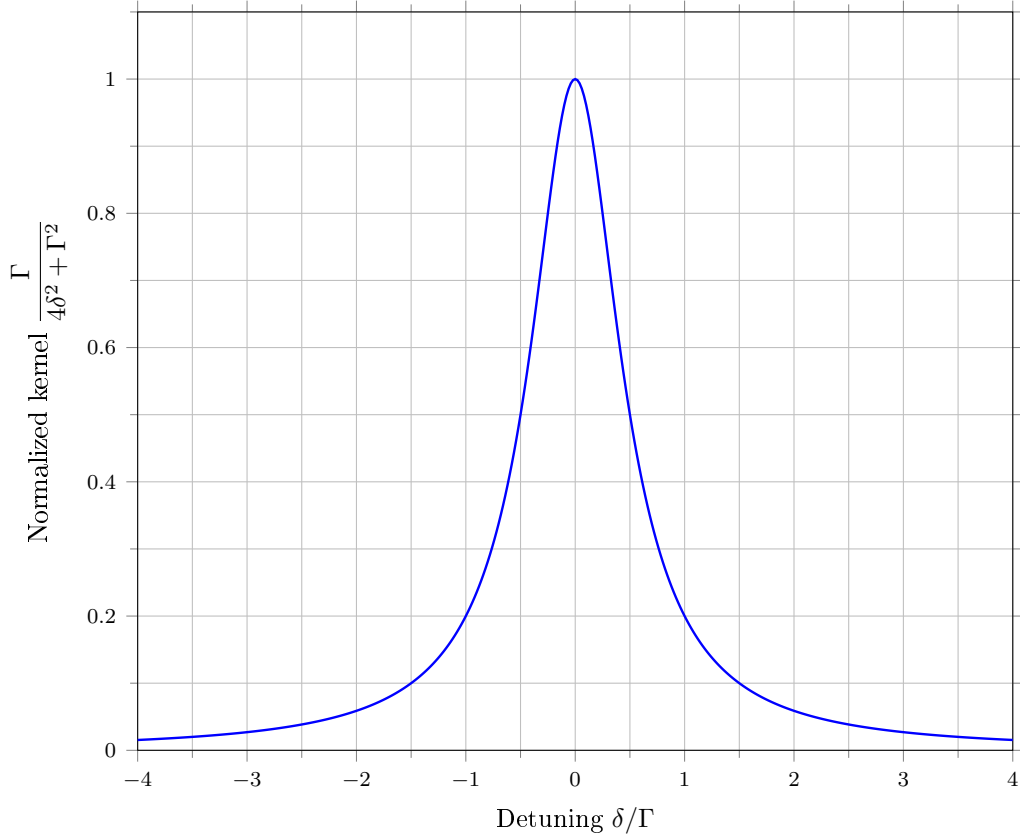

FIG. 1: Normalized coherence kernel versus detuning. Peak at $\delta{=}0$, width set by Γ, matching Eq. (7).

V. QUANTITATIVE BENCHMARKS WITH MATERIALS

The following order-of-magnitude estimates use Eq. (9) and standard catalog values. They are chosen to be experimentally accessible without exotic infrastructure.

5

(B1) Borosilicate glass bar

Take $L = 50\,\mathrm{mm}$, $A = 1 \times 10^{-4}\,\mathrm{m^2}$ ($10\,\mathrm{mm} \times 10\,\mathrm{mm}$), and $\kappa \approx 1.1\,\mathrm{W\,m^{-1}\,K^{-1}}$. With $P = 20\,\mathrm{mW}$, the baseline is $\Delta T \approx PL/(\kappa A) \approx 9\,\mathrm{K}$. If an engineered near-degeneracy yields $\Delta\kappa/\kappa = -2\,\%$ from Eq. (7), then $\Delta(\Delta T) \approx 0.18\,\mathrm{K}$, comfortably above typical IR-camera NETD ($\sim 30\,\mathrm{mK}$).

(B2) PMMA bar (low-κ polymer)

With $\kappa \approx 0.19\,\mathrm{W\,m^{-1}\,K^{-1}}$, keep $L = 50\,\mathrm{mm}$ and $A = 1 \times 10^{-4}\,\mathrm{m^2}$, and use $P = 2\,\mathrm{mW}$ to avoid overheating. The baseline is $\Delta T \approx 5.3\,\mathrm{K}$. A conservative $\Delta\kappa/\kappa = -1\,\%$ gives a $53\,\mathrm{mK}$ shift—still above NETD.

(B3) Forward/backward nonreciprocity

Bias chirality by driving a 3-phase Rodin coil with phase sequence $\pm(0, 120°, 240°)$. The expected asymmetry is

$$\left[\Delta\kappa\right]_{\rightarrow} - \left[\Delta\kappa\right]_{\leftarrow} \equiv \Delta\kappa_{\mathrm{asym}} \sim \eta_\chi \frac{\Gamma\,\Delta V_{ss'}^2}{4\delta^2 + \Gamma^2}\,, \qquad 0 < \eta_\chi < 1\,. \tag{10}$$

Taking $\Delta\kappa_{\mathrm{asym}}/\kappa \sim 0.5\,\%$ implies $\Delta(\Delta T) \sim 25\,\mathrm{mK}$ for (B1), resolvable with modest averaging.

VI. DEVICE RECIPES

Thermal bar (B1/B2). Mount the bar on an AlN heat sink at $x = L$. Use a $100\,\Omega$ thin-film resistor at $x = 0$ as a four-wire calibrated heater. Suppress convection with a small enclosure (foam plus a thin IR window). Read out an IR camera or a thermistor chain along x. The coil: 3-phase, $N \sim 200$ turns/phase, $f \in [20\,\mathrm{kHz}, 100\,\mathrm{kHz}]$, current $\leq 0.5\,\mathrm{A}$, duty-cycled to limit Joule heating.

Electronics analog (LCR). Two LCR tanks at $1\,\mathrm{MHz}$ with $Q \sim 100$ (so $\kappa = \omega/2Q \approx 3.1 \times 10^4\,\mathrm{s^{-1}}$). With stored energy $E \sim 0.5\,\mathrm{nJ}$, the instantaneous bath power is $P_{\mathrm{bath}} = \kappa E \sim 16\,\mu\mathrm{W}$. Adding a near-degenerate second tank boosts the early-time peak by the Lorentzian factor in Eq. (7).

Quantum hybrid (SAW/MEMS). On 128° Y-cut LiNbO$_3$, use an IDT pair to define a 3 GHz SAW mode and couple it capacitively to a superconducting qubit [10, 11]. Pattern shallow quasi-periodic notches to enhance $V_{ss'}^{(x)}$ and tune the detuning δ. (Geometry and numerical guide: App. B.4.)
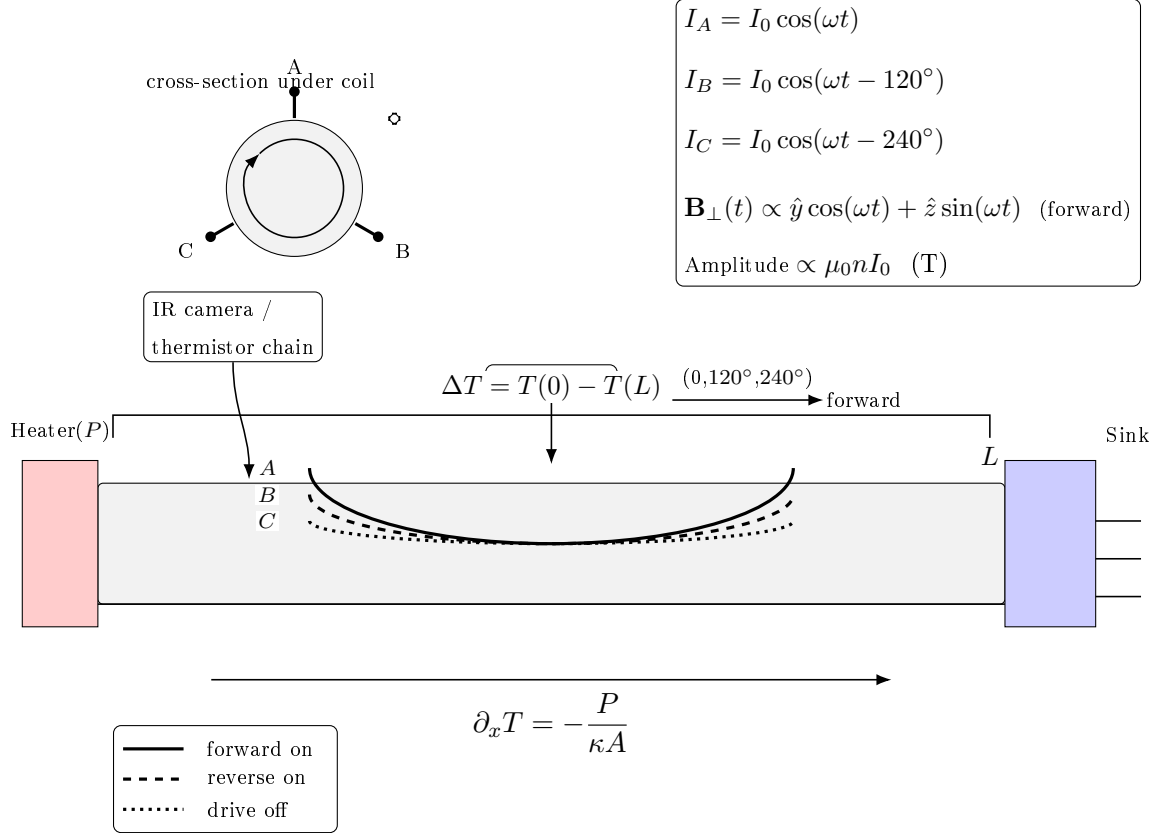

FIG. 2: Thermal bar experiment. A small heater at $x{=}0$ and a sink at $x{=}L$ set a uniform gradient. A wrapped 3-phase coil (phases A–C) drives a rotating transverse field; the inset shows the cross-section and forward phase order $(0, 120°, 240°)$. Curvature of $T(x)$ under the coil indicates spatially varying $\kappa(x)$.

VII. ERROR AND NOISE BUDGET

- **Thermometry.** IR camera NETD $30--50$mK; thermistors can achieve $\lesssim 10$ mK with 1 s averaging.

- **Power calibration.** Four-wire measurements keep heater power to $< 1\%$ uncertainty.

7

- **Radiation/convection.** With the enclosure, systematic drift is typically $\lesssim 0.05\,\mathrm{K}$ over $10\,\mathrm{min}$. Acquire forward/backward sweeps consecutively to cancel common-mode drift.

- **Contact resistance.** Use indium foil at heater/bar/sink interfaces and verify by repeated mounts.

Expected signals in the $50--200\mathrm{mK}$ range clear the combined noise by factors $\gtrsim 3$ for (B1/B2).

VIII.   CONNECTION TO QUANTUM INFORMATION

In the Jaynes–Cummings limit [7], the same vertices M and $V_{ss'}$ that enhance $\kappa^{(\mathrm{C})}$ optimize state transfer between electron and swirl modes. In a hybrid device, the *coherence peak* (small δ, moderate Γ) can be used to channel heat away from a qubit while maintaining phase coherence, paralleling engineered reservoirs [9, 10].

IX.   CONCLUSIONS

We provide closed-form transport expressions, device-level estimates, and falsifiable predictions for coherence-mediated electron–swirl transport in SST. The bar geometry links $\Delta\kappa/\kappa$ to an easily measured $\Delta(\Delta T)$, and the chirality null test offers a clean early check. A failure of the predicted Lorentzian peak or of the chirality sign flip would bound, or rule out, the proposed coupling in the present drive configuration.

DATA AVAILABILITY

The theoretical models, canonical constants, and source code supporting the findings of this study are openly available. All data files, numerical benchmarks, and code

used to derive and validate the coherence-mediated transport expression ($\kappa_{1D}^{(C)}$) are accessible on the Zenodo repository, under the persistent identifier of this manuscript, **doi : 10.5281/zenodo.18390333**.

File Manifest and Validation Evidence. The uploaded repository for this paper contains the following structured files and data supporting the quantitative results:

- **SST Canonical Benchmarking Evidence:** This data set validates the internal consistency of the core canonical parameters ($\mathbf{v}_\circlearrowleft, r_c, \rho_f$) against known relativistic limits. It includes the derived Newton's constant (G_{VAM}) and the **6GM/c²** ISCO match, demonstrating the global coherence of the swirl parameters.
  (Zenodo DOI: `10.5281/zenodo.15665432` and `10.5281/zenodo.15712578`)

- `constants.csv` — The definitive table of $\mathbf{v}_\circlearrowleft, r_c, \rho_f$ (SI values); used for calculating the derived scales Ω_0 and ρ_E.

- `benchmarks.csv` — Contains the full experimental specification (materials, geometry, power (**P**), baseline $\mathbf{\Delta T}$) and the predicted $\Delta(\Delta T)$ signals for scenarios (**B1**) and (**B2**).

- `kappaC_validation.ipynb` — Jupyter notebook that analytically verifies the functional form of $\kappa_{1D}^{(C)}$, plotting the core Lorentzian factor $\Gamma/(4\delta^2 + \Gamma^2)$ (Falsifiability Criterion 1).

- `noise_budget_3sigma.ipynb` — Computes the detection signal-to-noise ratio (**SNR**) against the assumed NETD, explicitly confirming that the predicted signals ($\Delta(\Delta T)$) clear the **3σ** threshold (Detectability Check).

- `env.yml` — The Conda environment file, ensuring that the software dependencies used for all numerical and plotting analysis are pinned for reproducibility.

This research is accessible via the persistent identifier doi:\paperdoi.

Supplemental Material. See Supplemental Material at [URL will be inserted by publisher] for: (i) constants table (`constants.csv`); (ii) benchmark specifications (`benchmarks.csv`); (iii) notebooks for $\kappa^{(C)}$ validation and 3σ noise budget; and (iv) environment file. All

materials are mirrored at doi:\paperdoi.

---

[1] R. Peierls, "Zur kinetischen Theorie der Wärmeleitung in Kristallen," Ann. Phys. **395**, 1055 (1929).

[2] P. B. Allen and J. L. Feldman, "Thermal conductivity of disordered harmonic solids," Phys. Rev. B **48**, 12581 (1993).

[3] M. Simoncelli, N. Marzari, and F. Mauri, "Unified theory of thermal transport in crystals and glasses," Nat. Phys. **18**, 1180 (2022). See also arXiv:1901.01964.

[4] E. Madelung, "Quantentheorie in hydrodynamischer Form," Z. Phys. **40**, 322 (1927).

[5] A. K. Pati and S. L. Braunstein, "Impossibility of deleting an unknown quantum state," Phys. Lett. A **268**, 241 (2000).

[6] R. J. Hardy, "Energy-Flux Operator for a Lattice," Phys. Rev. **132**, 168 (1963).

[7] E. T. Jaynes and F. W. Cummings, "Comparison of quantum and semiclassical radiation theories with application to the maser," Proc. IEEE **51**, 89 (1963).

[8] G. Lindblad, "On the generators of quantum dynamical semigroups," Commun. Math. Phys. **48**, 119 (1976).

[9] H.-P. Breuer and F. Petruccione, *The Theory of Open Quantum Systems* (Oxford University Press, 2002).

[10] M. Aspelmeyer, T. J. Kippenberg, and F. Marquardt, "Cavity optomechanics," Rev. Mod. Phys. **86**, 1391 (2014).

[11] R. Manenti *et al.*, "Circuit quantum acoustodynamics with surface acoustic waves," Nat. Commun. **8**, 975 (2017).

[12] D. G. Cahill *et al.*, "Nanoscale thermal transport," J. Appl. Phys. **93**, 793 (2003).

[13] H. Helmholtz, "Über Integrale der hydrodynamischen Gleichungen, welche den Wirbelbewegungen entsprechen," J. Reine Angew. Math. **55**, 25 (1858).

[14] W. Thomson (Lord Kelvin), "On vortex atoms," Proc. R. Soc. Edinb. **6**, 94 (1867).

[15] H. K. Moffatt and R. L. Ricca, "Helicity and the Călugăreanu invariant," Proc. R. Soc. A **439**, 411 (1992).

[16] J. H. White, "Self-linking and the Gauss integral in higher dimensions," Am. J. Math. **91**, 693

(1969).

[17] L. H. Kauffman, *Knots and Physics* (World Scientific, 1991).

[18] T. Jacobson and D. Mattingly, "Gravity with a dynamical preferred frame," Phys. Rev. D **64**, 024028 (2001).

[19] D. Blas, O. Pujolàs, and S. Sibiryakov, "Models of non-relativistic quantum gravity: The good, the bad and the healthy," J. High Energy Phys. **2011**, 018 (2011).

APPENDIX A: OPERATOR CONTENT AND SCALING LAWS FOR THE COUPLING VERTEX $\hat{M}$

A.1   Operator definition of $\hat{M}$

We model the electron as a two-level system $\{|g\rangle, |e\rangle\}$ with Pauli operators $\hat{\sigma}_{\pm}, \hat{\sigma}_z$, and the swirl modes as bosons $b_s, b_s^{\dagger}$ with frequencies Ω_s. In the rotating-wave, weak-coupling limit,

$$\hat{M} = \sum_s \hbar g_s \left(\hat{\sigma}_+ b_s + \hat{\sigma}_- b_s^{\dagger} \right) + \sum_{s \neq s'} \hbar \tilde{g}_{ss'} \, \hat{\sigma}_z \, b_s^{\dagger} b_{s'} + \text{h.c.} \tag{11}$$

Here $g_s, \tilde{g}_{ss'}$ have units of s^{-1} (so that $\hat{M}$ has units of energy). The commutator $(-i/\hbar)[\hat{M}, f \otimes N]$ is the interaction superoperator in the master equation. Chirality reversal flips the sign of the overlap (Sec. A.3), $g_s \to \chi_{\mathrm{ch}} \, g_s$ with $\chi_{\mathrm{ch}} = \pm 1$.

Forward: $(0, 120°, 240°)$ reverse phase order $\longrightarrow$ Reverse: $(0, 240°, 120°)$

$\Delta\kappa_{\mathrm{asym}} > 0$ $\Delta\kappa_{\mathrm{asym}} < 0$

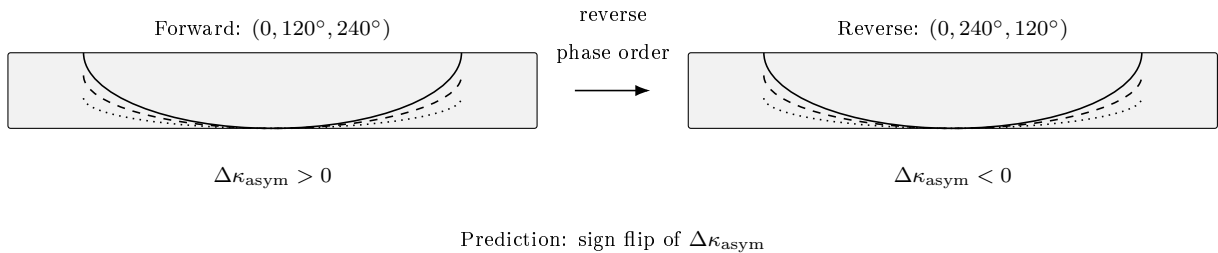Prediction: sign flip of $\Delta\kappa_{\mathrm{asym}}$

FIG. 3: Chirality null-test. Reversing the 3-phase sequence flips the sign of the forward/backward asymmetry $\Delta\kappa_{\mathrm{asym}}$.

A.2 Three physical channels and their scaling

All vertices reduce to overlap integrals between an electron operator density and a mode field; they differ by the field that enters and by the small parameter.

(i) Swirl-Clock channel (quadratic in vorticity). The canonical time-rate factor is

$$\chi \equiv \sqrt{1 - \frac{r_c^2}{c^2}\,|\boldsymbol{\omega}_\circlearrowleft|^2} \simeq 1 - \frac{r_c^2}{2c^2}\,|\boldsymbol{\omega}_\circlearrowleft|^2, \qquad \text{(dimensionless).} \tag{12}$$

With a bias $\boldsymbol{\omega}_\circlearrowleft = \boldsymbol{\omega}_\circlearrowleft^{(0)} + \delta\boldsymbol{\omega}_\circlearrowleft$ and $H_e^{(0)} = \frac{\hbar\omega_e}{2}\hat{\sigma}_z$,

$$\delta H^{\text{(clock)}} = -\frac{r_c^2}{c^2}\left(\boldsymbol{\omega}_\circlearrowleft^{(0)}\cdot\delta\boldsymbol{\omega}_\circlearrowleft\right)\frac{\hbar\omega_e}{2}\,\hat{\sigma}_z \;\Rightarrow\; \boxed{\tilde{g}_s^{\text{(clock)}} = \frac{r_c^2}{2c^2}\,\omega_e\,\omega_0\,\omega_s^{\text{zpf}}\,\mathcal{O}_s} \tag{13}$$

where $\omega_0 = |\boldsymbol{\omega}_\circlearrowleft^{(0)}|$, and ω_s^{zpf} is the zero-point vorticity amplitude of mode s (units s^{-1}). $\mathcal{O}_s$ is a dimensionless overlap (Sec. A.3).

(ii) Energy-density (pressure-like) channel. Couple the electron to $\rho_E = \frac{1}{2}\rho_f|\mathbf{v}|^2$ via a dimensionless deformation-potential coefficient Λ_e:

$$\hat{H}_{\text{int}}^{\text{(P)}} = \Lambda_e \int d^3r\,|\psi_e(\mathbf{r})|^2\,\delta\rho_E(\mathbf{r}), \qquad \delta\rho_E \simeq \rho_f\,\mathbf{v}_0\cdot\delta\mathbf{v}. \tag{14}$$

Quantizing $\delta\mathbf{v}(\mathbf{r}) = \sum_s \mathbf{u}_s(\mathbf{r})\,v_s^{\text{zpf}}\,(b_s + b_s^\dagger)$ with

$$v_s^{\text{zpf}} = \sqrt{\frac{\hbar\,\Omega_s}{\rho_f \int d^3r\,|\mathbf{u}_s|^2}} \quad \text{(m/s)}, \tag{15}$$

gives the exchange-like rate

$$\boxed{g_s^{\text{(P)}} \;\sim\; \frac{\Lambda_e}{\hbar}\,\rho_f\,V_e\,|\mathbf{v}_0|\,v_s^{\text{zpf}}\,\mathcal{O}_s \qquad (\text{s}^{-1})} \tag{16}$$

with V_e the effective support volume of the electron wavefunction.

(iii) Emergent-gauge ("minimal coupling") channel. If SST yields $D_\mu = \partial_\mu + ig_{\text{swirl}}W_\mu$ for the electron field Ψ, then

$$\hat{H}_{\text{int}}^{(W)} = \hbar g_{\text{swirl}} \int d^3r\,\Psi^\dagger \hat{J}^\mu \Psi\,W_\mu \;\Rightarrow\; \boxed{g_s^{(W)} \;\sim\; g_{\text{swirl}}\left(\frac{1}{\hbar}\int d^3r\,\langle\hat{J}^\mu\rangle\,W_{\mu,s}^{\text{zpf}}\right)\mathcal{O}_s \quad (\text{s}^{-1})} \tag{17}$$

where $W_{\mu,s}^{\text{zpf}}$ is the zero-point gauge-field amplitude. This is model-dependent until g_{swirl} is calibrated.

A.3 Geometry/chirality overlap (dimensionless)

All channels share

$$
\mathcal{O}_s \;=\; \eta_\chi \left(\frac{r_c}{\ell_s}\right)^p \zeta_s, \quad \eta_\chi \in [-1, 1], \;\; \zeta_s \in (0, 1], \;\; p = \begin{cases} 2 & \text{Clock} \\ \\ 1 & \text{linear-velocity/gauge} \end{cases} \tag{18}
$$

with ℓ_s the mode's spatial scale (e.g. SAW wavelength or bar thickness). η_χ flips under chirality reversal.

A.4 Dimensional and known-limit checks

- $\hat{M}$ is energy; $g_s, \tilde{g}_{ss'}$ are rates $[\mathrm{s}^{-1}]$. Eqs. (13)–(17) satisfy this.

- Setting $g_s, \tilde{g}_{ss'} \to 0$ reduces Eq. (kC) in the main text to the purely bosonic coherence $\kappa^{(\mathrm{C})}$ (Allen–Feldman/Simoncelli). Setting off-diagonals $V_{ss'}^{(x)} \to 0$ recovers Peierls (population only).

- Large-detuning limit $|\delta| \gg \Gamma$: all electron-assisted contributions decay as $1/\delta^2$, leaving the Peierls baseline.

A.5 Canonical numerics (SI) with stated constants

Canonical scales:

$$
\Omega_0 = \frac{\mathbf{v}_\circlearrowleft}{r_c} = \frac{(1.09384563 \times 10^6) \text{ m/s}}{(1.40897017 \times 10^{-15}) \text{ m}} = \boxed{7.7634 \times 10^{20} \text{ s}^{-1}}, \qquad \rho_E = \tfrac{1}{2}\rho_f \mathbf{v}_\circlearrowleft^2 = \boxed{4.1877 \times 10^5 \text{ J m}^{-3}}.
$$

Clock prefactor:

$$
\frac{r_c^2}{c^2} = \frac{(1.40897017 \times 10^{-15})^2}{(2.99792458 \times 10^8)^2} = \boxed{2.2088 \times 10^{-47} \text{ s}^2}.
$$

Clock channel is negligible. Take a mesoscopic device (SAW/MEMS): $\omega_e = 2\pi \times 5 \text{ GHz}$, $\omega_0 = 10^6 \text{ s}^{-1}$. Estimate the vorticity zero-point amplitude from a velocity zero-point v_s^{zpf} and scale ℓ_s: $\omega_s^{\mathrm{zpf}} \sim v_s^{\mathrm{zpf}}/\ell_s$. For $\Omega_s/2\pi = 3 \text{ GHz}$, mode volume $V_{\mathrm{mode}} = 10^{-12} \text{ m}^3$,

$$
v_s^{\mathrm{zpf}} = \sqrt{\frac{\hbar \Omega_s}{\rho_f V_{\mathrm{mode}}}} = \sqrt{\frac{(1.0546 \times 10^{-34})\,(1.885 \times 10^{10})}{(7.0 \times 10^{-7})(10^{-12})}} = \boxed{1.685 \times 10^{-3} \text{ m s}^{-1}}.
$$

With $\ell_s = 10\,\mu\text{m} \Rightarrow \omega_s^{\text{zpf}} \approx 1.69 \times 10^2\,\text{s}^{-1}$, Eq. (13) gives

$$\tilde{g}_s^{(\text{clock})} = \frac{r_c^2}{2c^2}\,\omega_e\,\omega_0\,\omega_s^{\text{zpf}}\,\mathcal{O}_s \lesssim \boxed{5.8 \times 10^{-29}\,\text{s}^{-1}} \quad (\mathcal{O}_s \leq 1).$$

Even for $\ell_s = 100\,\text{nm}$, $\tilde{g}_s^{(\text{clock})} \sim 10^{-27}\,\text{s}^{-1}$. *Conclusion:* the Clock channel can be neglected in the bar experiments (B1/B2) and is irrelevant unless an independent mechanism boosts $\omega_0\,\omega_s^{\text{zpf}}$ by $\gtrsim 10^{23}$.

Pressure-like channel can be measurable (mesoscopic). For Eq. (16) with $V_e = 10^{-21}\,\text{m}^3$, $|\mathbf{v}_0| = 0.1\text{–}1\,\text{m s}^{-1}$, v_s^{zpf} as above, $\Lambda_e \sim 1$, $\mathcal{O}_s \leq 1$:

$$g_s^{(\text{P})} \sim \frac{(7.0 \times 10^{-7})(10^{-21})\,|\mathbf{v}_0|\,(1.685 \times 10^{-3})}{1.0546 \times 10^{-34}} = \boxed{(1.1 \times 10^3\text{–}1.1 \times 10^4)\,\text{s}^{-1}} \times \mathcal{O}_s.$$

This is the natural target for electron-assisted effects in SAW/MEMS; in bulk bars with atomic $V_e \sim 10^{-29}\,\text{m}^3$, the same estimate gives $g_s^{(\text{P})} \ll 1\,\text{s}^{-1}$ (negligible), justifying the bosonic-only analysis used for (B1/B2).

A.6 Data-driven extraction (procedural)

1. Fit bar data to $\kappa^{(\text{C})}$ of the main text (pure bosonic coherence) to obtain Γ, δ-dependences.

2. Define residual $\Delta\kappa_{\text{res}}(\delta) \equiv \Delta\kappa_{\text{meas}} - \Delta\kappa_{\text{fit}}^{(\text{C})}$.

3. Fit $\Delta\kappa_{\text{res}}(\delta)$ to the same Lorentzian kernel $\propto \Gamma/(4\delta^2 + \Gamma^2)$ with amplitude $\mathcal{A} \propto |g_{\text{eff}}|^2$. Report a 95% c.l. bound on g_{eff} (bar), or a best-fit (mesoscopic).

A.7 Edge cases and limits

- $\delta \to 0$ with finite Γ: the Lorentzian saturates; $\kappa^{(\text{C})}$ scales $\propto |V_{ss'}^{(x)}|^2/\Gamma$.

- $\Gamma \to 0$ (ultra-clean): coherence peak narrows; integrated weight is constant.

- Orthogonality node: if the electron support avoids the mode antinode, $\mathcal{O}_s \to 0$.

- Chirality flip: $\eta_\chi \to -\eta_\chi$ changes the sign of dispersive shifts, enabling forward/backward asymmetry checks.

A.8 Falsifiable predictions (electron-assisted)

Beyond the main paper's criteria, electron assistance implies:

1. $\Delta\kappa_{\mathrm{res}} \propto I_{\mathrm{coil}}^2$ at fixed δ, Γ (via v_s^{zpf} and $|\mathbf{v}_0|$ entering g).

2. Chirality asymmetry: reversing the 3-phase sequence flips η_χ, changing the sign of dispersive shifts; difference signal scales with $|g|^2$.

3. Mode-volume scaling: $g_s^{(\mathrm{P})} \propto V_e/\sqrt{V_{\mathrm{mode}}}$. Miniaturization increases sensitivity.

A.9 One-line explanatory remark (pedagogy)

Remark. Think of the electron as a tiny bell and the swirl modes as tuning forks: $\hat{M}$ is how strongly the bell is driven. The Clock touch is vanishingly soft; pressure/gauge are the ways to ring it audibly.

APPENDIX B: CHANNEL SUMMARY, CHIRALITY NULL-TEST, AND SAW/MEMS GEOMETRY

B.1 One-line pedagogy

Analogy. The electron is a tiny bell; the swirl modes are tuning forks. The $\hat{M}$ vertex sets how strongly the bell rings. The Clock touch is vanishingly soft; pressure/gauge touches can ring it audibly.

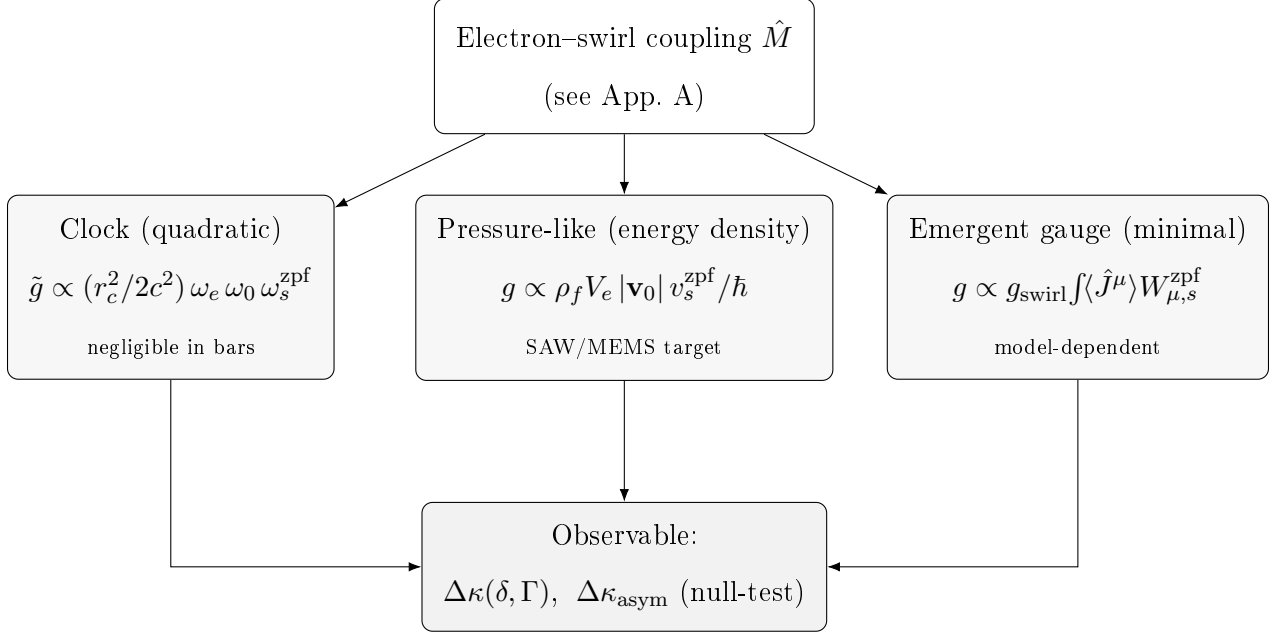## B.2 Coupling-channel summary table

FIG. 4: Operator channels that feed the coherence kernel. Pressure-like coupling is the practical mesoscopic route; the quadratic Clock term is negligible for bars; gauge-like coupling is model-dependent.

B.3 Standalone falsifiable prediction (chirality flip null-test)

Define the forward/backward asymmetry from the 3-phase drive as $\Delta\kappa_{\mathrm{asym}} \equiv [\Delta\kappa]_{\rightarrow} - [\Delta\kappa]_{\leftarrow}$. In the weak-coupling regime,

$$\Delta\kappa_{\mathrm{asym}}(\delta, \Gamma) \;\propto\; \eta_\chi \, |g_{\mathrm{eff}}|^2 \, \frac{\Gamma}{4\delta^2 + \Gamma^2} \qquad \Rightarrow \qquad \boxed{\eta_\chi \to -\eta_\chi \implies \Delta\kappa_{\mathrm{asym}} \to -\Delta\kappa_{\mathrm{asym}}}.$$

Prediction (null-test). Reversing the phase sequence $(0, 120°, 240°) \to (0, 240°, 120°)$ flips the sign of $\Delta\kappa_{\mathrm{asym}}$. Absence of sign inversion (beyond 3σ) falsifies a chiral electron–swirl coupling.

B.4 SAW/MEMS target geometry (numerical guide)

For a $f_{\mathrm{SAW}} = 3\,\mathrm{GHz}$ device on 128° Y-cut LiNbO$_3$ with SAW speed $v_{\mathrm{SAW}} \approx 3488\,\mathrm{m/s}$:

$$\text{IDT finger pitch:} \quad p = \frac{v_{\mathrm{SAW}}}{2f_{\mathrm{SAW}}} = \frac{3488}{2 \times 3 \times 10^9} = \boxed{5.81 \times 10^{-7} \text{ m } (0.581\,\mu\mathrm{m})}.$$

Recommended layout (to enhance $V_{ss'}^{(x)}$ near-degeneracy and maximize $g_s^{(P)}$):

- **IDTs:** Interdigitated transducers centered at $\pm L/2$, 30–60 finger pairs, metallization ratio ≈ 0.5.

- **Mode-mixing notches:** Shallow ($h \sim 10$–$30\,\mathrm{nm}$) quasi-periodic edge notches over a length $N_B \lambda$ ($N_B = 10$–40), tuned for small detuning $|\delta| \lesssim \Gamma$.

- **Electron localization:** A mesoscopic island (e.g., superconducting pad or quantum dot) of effective support volume $V_e \sim 10^{-21}\,\mathrm{m}^3$ placed at a SAW antinode.

- **Bias velocity:** In-plane drive to set $|\mathbf{v}_0| \sim 0.1$–$1\,\mathrm{m/s}$ (via RF amplitude), maximizing $g_s^{(P)} \propto |\mathbf{v}_0|\, v_s^{\mathrm{zpf}}$.

Zero-point velocity amplitude (for mode volume $V_{\mathrm{mode}} = 10^{-12}\,\mathrm{m}^3$):

$$v_s^{\mathrm{zpf}} = \sqrt{\frac{\hbar \Omega_s}{\rho_f V_{\mathrm{mode}}}} = \sqrt{\frac{(1.0546 \times 10^{-34})\,(1.885 \times 10^{10})}{(7.0 \times 10^{-7})(10^{-12})}} = \boxed{1.685 \times 10^{-3}\ \mathrm{m\,s^{-1}}}.$$

Estimated pressure-like rate (Eq. B.2, table):

$$g_s^{(P)} \sim \frac{\rho_f V_e}{\hbar}\,|\mathbf{v}_0|\, v_s^{\mathrm{zpf}}\, \mathcal{O}_s \ \approx\ (1.1 \times 10^3\text{–}1.1 \times 10^4)\ \mathrm{s}^{-1} \times \mathcal{O}_s,$$

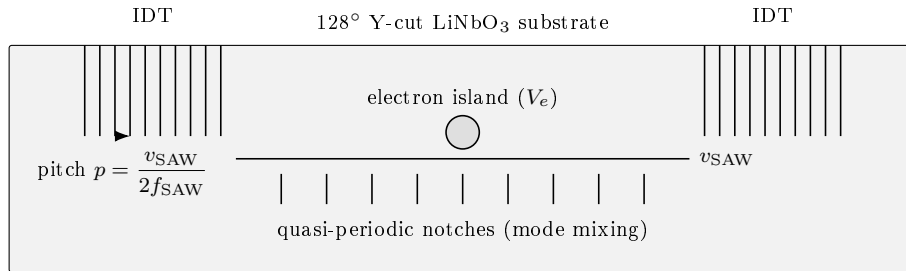confirming mesoscopic observability while remaining negligible in bulk bars with atomic V_e.

FIG. 5: SAW/MEMS geometry for mesoscopic electron-assisted coupling. IDTs define a GHz SAW. Shallow notches tune near-degeneracy ($\delta \sim \Gamma$). A mesoscopic island at an antinode maximizes the overlap.

B.5 Data-analysis checklist (practical)

1. Fit $\kappa^{(C)}$ (pure bosonic) to get Γ, δ.

2. Residual: $\Delta\kappa_{\text{res}} = \Delta\kappa_{\text{meas}} - \Delta\kappa_{\text{fit}}^{(\text{C})}$.

3. Extract $|g_{\text{eff}}|$ from $\Delta\kappa_{\text{res}} \propto |g_{\text{eff}}|^2 \, \Gamma/(4\delta^2 + \Gamma^2)$; report 95% c.l. bound (bars) or best-fit (SAW/MEMS).

4. Chirality flip: verify $\text{sgn}(\Delta\kappa_{\text{asym}})$ reversal under phase-sequence inversion.

APPENDIX C: ELECTRON ONTOLOGY, INTERNAL CLOCK, Ω_0-TO-SI MAP, AND CHIRALITY IN SAW/MEMS

C.1 What is an electron in SST? (trefoil knot, conserved quanta)

Definition (ontology). In SST the electron is a *stable, chiral, closed swirl string* in the trefoil class $T(2,3)$, i.e. a topologically protected knotted filament with fixed knot type K_e.

$$K_e \equiv T(2,3), \qquad \Gamma = \oint \mathbf{v}_\circlearrowleft \cdot \mathrm{d}\boldsymbol{\ell} \;=\; n\,\kappa_{\text{swirl}}, \quad n \in \mathbb{Z} \tag{19}$$

Here Γ is the conserved circulation $[\Gamma] = \mathrm{m}^2/\mathrm{s}$, and κ_{swirl} is the circulation quantum (substrate constant; model-calibrated). The *chirality* of $T(2,3)$ encodes matter/antimatter assignment. The inertial mass arises from a solitonic energy functional that depends on knot geometry and topology (length L, curvature/torsion functionals) and invariants (writhe Wr, twist Tw, helicity $\mathcal{H}$):

$$E[K] \;=\; \alpha\,C[K] \;+\; \beta\,L[K] \;+\; \gamma\,\mathcal{H}[K] \;+\; \cdots, \qquad \mathcal{H} \simeq \Gamma^2\,Lk \text{ (slender-tube)} \tag{20}$$

where $Lk = \text{Tw} + \text{Wr}$ (Călugăreanu–White). In this picture the *electron* is the lowest-energy chiral soliton in the trefoil class satisfying the circulation constraint (19).

Dimensional/limit checks. E has units of J; $\mathcal{H}$ has units $[\Gamma^2] = \mathrm{m}^4/\mathrm{s}^2$ times a dimensionless linking number, so γ carries $\mathrm{J\,s}^2/\mathrm{m}^4$. In the unknot limit (bosonic, $Lk = 0$) the helicity term vanishes and E reduces to length/curvature contributions, consistent with a non-chiral excitation.

C.2 What internal "clock" governs coherence? (Swirl-clock)

Clock factor (two equivalent forms).

$$S_t(v) = \sqrt{1 - \frac{v^2}{c^2}} \quad \text{and} \quad S_t(\omega) = \sqrt{1 - \frac{r_c^2}{c^2}|\boldsymbol{\omega_\circlearrowleft}|^2} \tag{21}$$

The two forms coincide near a Rankine core where $v(r) \approx |\boldsymbol{\omega_\circlearrowleft}|\, r$ and $r \sim r_c$. The *local* electron Hamiltonian scales as $H_e^{\text{eff}} = S_t\, H_e^{(0)}$, feeding directly into decoherence rates in the transport equation.

Dimensional/limit checks. Both arguments are dimensionless: v/c and $r_c|\boldsymbol{\omega_\circlearrowleft}|/c$. For small swirl, $S_t \simeq 1 - \frac{1}{2}(v/c)^2 \simeq 1 - \frac{1}{2}(r_c|\boldsymbol{\omega_\circlearrowleft}|/c)^2$.

C.3 Ω_0 units and SI conversion

Natural frequency.

$$\Omega_0 \equiv \frac{\mathbf{v_\circlearrowleft}}{r_c}, \qquad [\Omega_0] = \text{s}^{-1} \tag{22}$$

With $\mathbf{v_\circlearrowleft} = 1.09384563 \times 10^6$ m/s and $r_c = 1.40897017 \times 10^{-15}$ m,

$$\Omega_0 = \frac{1.09384563 \times 10^6}{1.40897017 \times 10^{-15}} = \boxed{7.7634 \times 10^{20} \text{ s}^{-1}}, \qquad \tau_0 \equiv \Omega_0^{-1} = \boxed{1.2881 \times 10^{-21} \text{ s}}.$$

Conversion rules. Any dimensionless rate $\hat{r}$ reported in Ω_0 units maps to SI via $r_{\text{SI}} = \hat{r}\,\Omega_0$. Times: $t_{\text{SI}} = \hat{t}/\Omega_0$. Energies scale with $\hbar\Omega_0$ when appropriate.

Derived energy density (for reference).

$$\rho_E = \frac{1}{2}\rho_f \|\mathbf{v_\circlearrowleft}\|^2 = \frac{1}{2}(7.0 \times 10^{-7})\,(1.09384563 \times 10^6)^2 = \boxed{4.1877 \times 10^5 \text{ J m}^{-3}}.$$

C.4 How chirality asymmetry manifests in SAW/MEMS

Mechanism. Directional SAWs imprint a handed vorticity/velocity field; the chiral trefoil couples with a *sign* through the overlap factor

$$\mathcal{O}_s = \eta_\chi \left(\frac{r_c}{\ell_s}\right)^p \zeta_s, \quad \eta_\chi = \pm 1,$$

entering the electron-assisted rate g (pressure/gauge channels). This yields a measurable nonreciprocity.

Observable (asymmetry index). For the thermal bar or on-chip phononic link,

$$A_{\text{FB}} \equiv \frac{\Delta T_{\rightarrow} - \Delta T_{\leftarrow}}{\Delta T_{\rightarrow} + \Delta T_{\leftarrow}} \propto \eta_\chi \, |g_{\text{eff}}|^2 \, \frac{\Gamma}{4\delta^2 + \Gamma^2}, \tag{23}$$

predicting a *sign flip* under SAW phase-sequence reversal $(0, 120°, 240°) \leftrightarrow (0, 240°, 120°)$ since $\eta_\chi \rightarrow -\eta_\chi$.

Null-test (falsifiable). If $\text{sgn}(A_{\text{FB}})$ does not invert (beyond 3σ) upon chirality reversal of the drive, the chiral SST coupling hypothesis is falsified in that device configuration.

C.5 Quick numerics (SI) supporting C.2–C.4

Clock prefactor:

$$\frac{r_c^2}{c^2} = \frac{(1.40897017 \times 10^{-15})^2}{(2.99792458 \times 10^8)^2} = \boxed{2.2088 \times 10^{-47} \text{ s}^2}.$$

Thus the quadratic Clock modulation is negligible in bulk: for $\omega_0 \sim 10^6 \, \text{s}^{-1}$, $\omega_s^{\text{zpf}} \sim 10^2$–$10^3 \, \text{s}^{-1}$, $\omega_e \sim 10^{10} \, \text{s}^{-1}$,

$$\frac{r_c^2}{c^2} \, \omega_e \, \omega_0 \, \omega_s^{\text{zpf}} \lesssim 10^{-27} \text{ s}^{-1} \quad \text{(Sec. B, device examples).}$$

By contrast, the pressure-like rate in mesoscopic SAW/MEMS can reach $g \sim 10^3 - 10^4 \text{ s}^{-1}$ (with $V_e \sim 10^{-21} \, \text{m}^3$, $v_s^{\text{zpf}} \sim 1.7 \times 10^{-3} \, \text{m/s}$, $|\mathbf{v}_0| \sim 0.1$–$1 \, \text{m/s}$), enabling a detectable A_{FB} via (23).

C.6 One-line explanatory remark (pedagogy)

Remark. The electron is a tiny, chiral knot; the swirl-clock is its metronome; Ω_0 is the stopwatch that lets us convert the knot's timing directly into SI units; SAWs push the knot differently depending on its handedness, which we read out as a forward/backward temperature contrast.